GAS FLOWS WITHIN TURNING SECTIONS

R. PLATFOOT

Fuel and Combustion Scientific Services, Electricity Commission of New South Wales, Electricity House, Sydney, NSW 2000, Australia

AND

C. A. J. FLETCHER

Department of Mechanical Engineering, University of Sydney, Sydney, NSW, Australia

ABSTRACT

An alternative algorithm has been developed for computing the behaviour of flows within arbitrary ducts and channels. This technique requires a small number of downstream marches in the primary flow direction, employing, on each march, numerically efficient procedures originally developed for a single sweep non-elliptic flow solver. The multiple sweeps allow the capture of effects such as upstream pressure influences and streamwise recirculation. The energy equation is also solved to allow for varying heat transfer between the fluid and the boundary walls. The numerical work is further complicated by considering flows within turning sections of ducts which demonstrate large transverse velocities and consequent distortion of the primary flow. The computations are validated by comparison with a number of fluid/heat transfer experiments. The majority of these are taken from studies of turning flows within circular arc ducts which display the various pressure and transverse flow phenomena for which this new algorithm was initially developed to represent.

KEY WORDS   Circular arc ducts   Gas flows   Turning sections

INTRODUCTION

Internal flows within turning sections are of widespread industrial relevance. Typically, these types of flows demonstrate adverse streamwise pressure gradients, strong upstream influences which propagate against the direction of flow, large transverse velocities and, possibly, streamwise recirculation. Predicting the behaviour of the fluid is further complicated by varying heat transfer to the perimeter walls leading to density gradients within the bulk flow. Contemporary computational solvers for these classes of flows rely on global or fully three-dimensional iteration[1-3], particularly to simulate downstream conditions propagating against the direction of flow. More numerically efficient marching algorithms have been applied to a limited number of these problems[4-6]. The current contribution is the development of an otherwise non-elliptic solver via the framework of repeated forward sweeps. This allows for forward and backward pressure influences, streamwise recirculation and other 'elliptic' effects. A high level of computational efficiency is still possible with this approach compared with the full three-dimensional iterative techniques, thus allowing the use of much finer grids for the same overall execution times.

The types of flow situations described above are especially relevant to many heat exchanger applications, particularly in the power industry where hot working fluids typically pass through cooler channels—gas flows in boilers, steam within turbine passes, feed heaters etc. The greater majority of the flows are contained within turning passages so that the significant secondary

flows are rotational, being induced by the local curvature. For this reason, the non-elliptic algorithm developed by Briley and McDonald[7] is employed as the basis for the current work. We briefly describe pertinent aspects of this algorithm and demonstrate the various departures and enhancements due to embedding it within the multiple sweep framework. The results to date have been principally obtained for validation of the new code. Hence the comparisons are with experimental studies of circular arc ducts for which a body of detailed measurements is available.

NUMERICAL DEVELOPMENT

The current algorithm is developed in a curvilinear orthogonal coordinate system which is compatible with a boundary fitted mesh. This allows the solution of flows in a broad range of duct and channel configurations with only small errors occurring due to minor departures from orthogonality by the computational mesh[8]. *Figure 1* describes the transformation of the physical domain to a regular computational grid upon which finite differences are used to represent partial differentials. In this Figure the streamwise or marching direction for the algorithm is clearly identified. The transverse placement of mesh points is boundary clustered in each of the transverse directions in the physical domain following Roberts'[9] algebraic transformation:

$$\eta = 0.5 \pm 0.5\left(1 + \frac{\ln\left(\dfrac{b - d_\eta + |(d_\eta - y)|}{b + d_\eta - |(d_\eta - y)|}\right)}{\ln\left(\dfrac{b + d_\eta}{b - d_\eta}\right)}\right)$$

$$b = \frac{d_\eta}{\sqrt{1 - \beta}}$$

where β is the equivalent boundary layer thickness (normally set at 0.2), y and η are the physical and computational coordinates as indicated on *Figure 1*, and d_η is the half duct width. The subsequent transformation process or generation of metrics allows for the clustering to provide a regular distribution of mesh points, in the computational domain, for all directions. In this manner, constant difference intervals are allowed such that $\Delta\xi = (1/L_\xi - 1)L_\xi$ being the number of mesh points in the ξ direction.

The mesh generation in the physical domain is based on placing planar surfaces, either flat or curved, along the primary axis of the duct as indicated on *Figure 1*. The planes are free to vary in cross-sectional area to allow for converging/diverging duct walls. The positioning of the transverse planes was initially achieved by fitting analytic functions to ensure that solution points
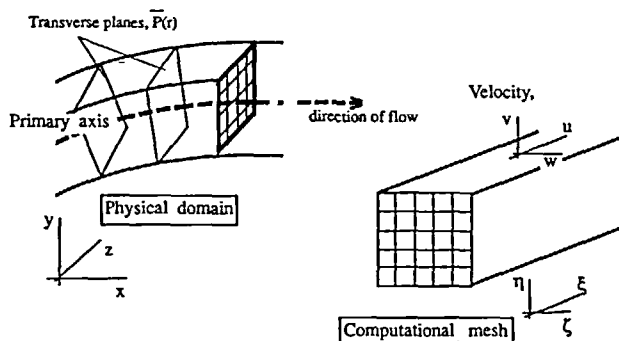

Figure 1 Computational mesh transformation

could be aligned with planes of measurement points when simulating experimental or field situations. Alternatively, the planes may be placed using algebraic techniques such as the multisurface method proposed by Eiseman[10]:

$$\text{for} \quad \bar{P}_k \leqslant \bar{P} \leqslant \bar{P}_{k+1}$$

$$\bar{P}(r) = \bar{P}_k + G_k(r)[\bar{P}_{k+1} - \bar{P}_k] + G_{k+1}(r)[\bar{P}_{k+2} - \bar{P}_{k+1}]$$

where $\bar{P}_k$ are the control planes which define the geometry, G_k are the respective algebraic blending functions and $\bar{P}(r)$ are the transverse solution planes which mesh the geometry. The control planes are independently defined and spaced in a cyclic process governed by monitoring mesh diagnostics such as smoothness of the streamwise metrics included in various terms of the governing equations. This multisurface method provides superior mesh smoothness, particularly for straight to curved transitions; but at the expense of slight inaccuracies in boundary control between the control planes.

The governing equations included the conservation of continuity, momentum and energy. The Briley and McDonald algorithm[7] is based on the change of dependent variables for certain transverse velocity terms. This is achieved by splitting the secondary velocities, v and w, into rotational and potential terms:

$$v = \frac{1}{h_\eta} \frac{\partial \phi}{\partial \eta} + \frac{1}{h_\xi h_\zeta \rho} \frac{\partial h_\xi \psi}{\partial \zeta}; \quad w = \frac{1}{h} \frac{\partial \phi}{\partial \zeta} - \frac{1}{h_\xi h_\eta \rho} \frac{\partial h_\xi \psi}{\partial \eta}$$

where ϕ is the secondary potential and ψ is effectively a transverse flow stream function. The purpose of this splitting is to omit selected potential terms in the transverse momentum equations on an order-of-magnitude basis. This causes the system of equations to be solved at any plane $\bar{P}(r)$ to be well posed as an initial value problem in the marching direction, and hence amenable to solution by non-elliptic procedures[8]. Briefly, the governing equations are listed in their order of solution:

$$(\mathbf{V} \cdot \Delta_t)\Omega_\xi - (\Omega_\xi \cdot \Delta_t)\bar{\mathbf{V}} = Re^{-1}\Delta_t^2 \Omega_\xi$$

$$\Delta_t^2 h_\xi \psi = -\Omega_\xi$$

$$\Delta_t^2 \Delta p = -\Delta_t \cdot (\mathbf{V} \cdot \Delta_t)\bar{\mathbf{V}}$$

$$\rho(\mathbf{V} \cdot \Delta_t)u + \frac{\partial p}{\partial \xi} = Re^{-1}\Delta_t^2 u$$

$$\frac{\partial \rho u}{\partial \xi} + \Delta_t^2 \phi = 0$$

$$\rho(\mathbf{V} \cdot \Delta_t)T = (PrRe)^{-1}\Delta_t^2 T$$

where $\bar{\mathbf{V}}$ is the reduced velocity vector with potential contributions omitted from the transverse terms, v and w. $\Omega = \xi \cdot (\Delta_t \times \mathbf{V})$ is the streamwise vorticity, T is the fluid temperature and Δ_t is the transformed differential operator including metric terms. Additional curvature terms have not been indicated above but the full form of the equations and their derivation may be obtained from References 4 and 7.

The order of solution is based on successive transverse planes, $\bar{P}(r)$ above, located along the primary axis in the direction of the main flow. At the completion of one march through the flow domain, the procedure is repeated from the inlet until the pressure and velocity fields converge to a stable solution, unchanging from one march to the next. Hence two levels of convergence are implicit in the procedure: the first follows from the immediate solution at each location on any one march, and the second from one forward sweep to the next. Typically, the convergence criteria is identical for both processes and, currently, a sweep wise convergence of less than 1×10^{-4} is achieved within ten to fifteen marches for flows with minor recirculation.

At each transverse plane a series of partial differential equations are solved to provide velocity, pressure and temperature primitives. The structure of these equations and their order of solution follows Briley and McDonald's parabolic or single sweep procedure. All transverse partial differentials are represented as second order centre differences while, normally, all streamwise differentials are included as first order forward or backward differences. The exceptions to the latter include the treatment of the streamwise pressure gradient and the inclusion of the streamwise diffusion term, both in the axial momentum equation. The principal modifications made to the single sweep algorithm are the inclusion of upstream influences, as calculated during the previous sweep, the explicit calculation of streamwise diffusion and the use of the previous sweeps' velocities for the streamwise convective operator, $u(\partial u/\partial \xi)$.

The pressure, p is split into a static component, $\bar{p}$ governed by the mass flux requirement, $\iint \rho u \, dA = \dot{Q}$, ($\dot{Q}$ is the mass flow) and a transverse correction, Δp, provided from the Poisson equation indicated above for pressure. The streamwise pressure gradient term in the axial momentum equation is then discretized as:

$$\frac{\partial p}{\partial \xi} = \frac{\bar{p}_i - p_{i-1}}{\Delta \xi} + (1-\beta)\frac{\Delta p_i^n - \Delta p_{i-1}^n}{\Delta \xi} + \beta \frac{\Delta p_{i+1}^{n-1} - \Delta p_i^n}{\Delta \xi}$$

where n is the sweep indicator and i the axial locator. β is a relaxation coefficient which linearly increases, typically over the first five sweeps, from zero on the first downstream march to a steady value of:

$$\beta = \frac{\hat{\beta}}{1+\gamma}$$

$$\gamma = \frac{\sqrt{(x_{i+1}-x_i)^2 + (y_{i+1}-y_i)^2 + (z_{i+1}-z_i)^2}}{\sqrt{(x_i-x_{i-1})^2 + (y_i+y_{i-1})^2 + (z_i-z_{i-1})^2}}$$

$\hat{\beta}$ is normally set to approximately 0.8. This development follows from summing the Taylor series expansion of both the forward and backward pressure differences similar to their addition in the momentum equation. The above form ensures that otherwise numerically destabilizing second order terms will be suppressed[11].

The velocity terms in the convective operators are normally obtained from the results of the previous march. This formulation is compared below with the original Briley and McDonald approximation which was retained for the initial solution sweep:

First sweep:

$$u\frac{\partial u}{\partial \xi} = \begin{cases} u_{i-1}\dfrac{u_i-u_{i-1}}{\Delta \xi} & u_{i-1} \geqslant 0 \\ 0 & u_{i-1} < 0 \end{cases}$$

Sweep n:

$$u\frac{\partial u}{\partial \xi} = \begin{cases} u_i^{n-1}\dfrac{u_i-u_{i-1}}{\Delta \xi} & u_i^{n-1} \geqslant 0 \\ u_i^{n-1}\dfrac{u_{i+1}^{n-1}-u_i^n}{\Delta \xi} & u_i^{n-1} < 0 \end{cases}$$

It may be observed that the multiple sweep process allows a more accurate representation of the convective terms as convergence is approached ($u_i^{n-1} \to u_i^n$). In addition, upwinding is also implemented in areas of recirculation rather than the FLARE type approximation $[u(\partial u/\partial \xi)=0]$[12] employed by some contemporary single march schemes[13]. Future development of the algorithm should also allow the first order upwinding to be superseded by more accurate forms less susceptible to error by numerical diffusion.

In a similar treatment to the above, the downstream terms required to represent the streamwise diffusion term in the axial momentum equation are represented by the solution obtained during the previous forward sweep

$$\frac{\partial^2 u}{\partial \zeta^2} = \frac{u_{i+1}^{n-1} - 2u_i^{n-1} + u_{i-1}^n}{\Delta \zeta^2}$$

This explicit treatment of the diffusion term allows it to be included as a source term rather than providing additional contributions to be implicitly solved as part of the current sweep solution. The inclusion of streamwise diffusion is numerically desirable given that the solution procedures employed in the current form of the code are approximate factorization techniques requiring the reduction of tridiagonal matrices[14]. Providing the sweep-wise convergence is consistent, such that each sweep does not produce an order of magnitude correction to the relevant primitives, the streamwise diffusion term provides a positive addition to the diagonal terms of the augmented matrices as well as a subsequent improvement in accuracy. The former has a well documented benefit of stabilizing the solution process and avoiding perturbations in the solution which are often mesh associated[15].

An algebraic mixing length turbulence model has been developed with the present code. Its algorithm is a three-dimensional adaption of Cebeci and Smith's proposal[16] incorporating the various influences from all of the bounding walls. The system of equations which describe this model include:

$$l = \kappa \mathscr{L} [1 - \exp(-t^+/A^+)]$$

$$t^+ = \mathscr{L} Re\, u_r; \quad u_r = \sqrt{\frac{\tau_w}{\rho} + \frac{\partial p}{\partial \zeta} \frac{\mathscr{L}}{\rho}}$$

$$\tau_w = \alpha \left[\frac{1}{\eta^{*2}} \tau_{w-\eta} + \frac{1}{\zeta^{*2}} \tau_{w-\zeta} \right]$$

$$\alpha = \left[\frac{1}{\eta^{*2}} + \frac{1}{\zeta^{*2}} \right]; \quad \eta^* = \min(\eta, 2d_\eta - \eta); \quad \zeta^* = \min(\zeta, 2d_\zeta - \zeta)$$

κ is the von Karman constant, A^+ is 26.0 and the final wall stress term used to calculate the friction velocity, u_r is an inverse square addition of the wall stresses calculated on each of the two neighbouring walls in the η and ζ directions. The length scale, $\mathscr{L}$, is the Buleev mixing length for which the computationally efficient form used by Arnal and Cousteix[17] is employed:

$$\mathscr{L} = \frac{2\eta^* \zeta^*}{(\eta^{*2} + \zeta^*)^{\frac{1}{2}} + \eta^* + \zeta^*}$$

For internal flows, the otherwise simple Buleev mixing length is damped using a modification of the Van Driest approach as recommended by Cebeci and Chang[18]. In this application, there is no requirement for an 'outer model' providing the flow is well developed. The damped mixing length, l, is then incorporated into the eddy viscosity calculation:

$$v_t = l^2 \left[\left(\frac{1}{h_\eta} \frac{\partial u}{\partial \eta} \right)^2 + \left(\frac{1}{h_\eta} \frac{\partial w}{\partial \eta} \right)^2 + \left(\frac{1}{h_\zeta} \frac{\partial u}{\partial \zeta} \right)^2 + \left(\frac{1}{h_\zeta} \frac{\partial u}{\partial \zeta} \right)^2 \right]^{\frac{1}{2}}$$

$$\mu_t = \mu_m + Re\, v_t$$

where μ_t is the effective viscosity, μ_m is the molecular viscosity (normalized to 1.0) and v_t, the turbulent kinematic viscosity. Using the three-dimensional form above allows potentially large secondary velocity gradients to influence the turbulence field, particularly for the type of flow situations being addressed by the current work.

RESULTS

The results are presented in four stages: laminar isothermal flow in a circular arc duct, laminar/turbulent flow in a straight duct, turbulent flow in the same circular arc duct and, finally, laminar flow in the circular arc duct but with heated walls. These comparisons form a significant part of the validation of the numerical development as it has progressed to date. The primary objective of this ordering is to demonstrate the complexity of turning flows, the smoothing contribution provided by turbulence and the distorted heating of the fluid within a turning section. The computational meshes used to represent the circular arc duct were generated using the multisurface technique described earlier in this paper. The greatest departure from orthogonality occurred at the transitions between straight and curved sections with a peak angular error of 3.5°. Aspect ratios of curvilinear cells was held below 2.8 and sufficient streamwise fineness was achieved with 71 transverse planes aligned in the marching direction. The transverse meshing was typically 31×16 although some testing was carried out with a transverse mesh of 41×21 for the purposes of evaluating mesh refinement.

Figure 2 compares the current results with those computed by Rhie[1] and Humphrey *et al.*[20] plus the experimental measurements provided by the latter group. The current results were obtained following sixteen downstream marches although the greater proportion of the flow field achieved convergence after nine sweeps. The critical region which required further iterations to acheive a steady solution was associated with a small recirculation zone encountered near the inlet to the bend. The inlet plane results (0°) have been slightly misaligned to demonstrate the marginal recirculation at the 4° plane predicted by the current algorithm which is in keeping with experimental observations. Separation was first detected just prior to the 0° plane of the bend and negative streamwise velocities were predicted through to 14° within the turn. This differs slightly from the results reported by Rhie who predicted negative streamwise velocities at the 30° plane using the FLARE approximation. The starting flow for the current work is also plotted on *Figure 2* to demonstrate the movement of the flow within the initial straight section preceding the bend. This distortion of the streamwise velocity distribution is induced by the upstream pressure influences identified earlier in this paper. The 4° plane result for the converged
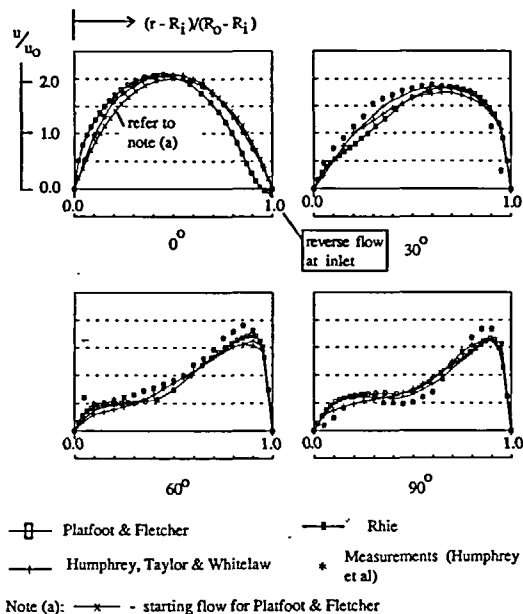

Figure 2   Laminar flow ($Re = 790$) in a circular arc duct with $R_i/R_o = 1.8/2.8$

solution significantly differs from that calculated on the first march of the multi-sweep process with the latter closely following the starting flow profile.

As the fluid moves through the turning section, the distortion of the streamwise flow may be observed. Generally, the various numerical predictions qualitatively match the experimental measurements, although some slight discrepancies are present in all three results. This was attributed to poor mesh refinement[20] in the earlier papers. The current work evaluated numerical results on both 71 (streamwise) × 16 and 71 × 41 × 21 meshes; in both cases a symmetry condition was applied to allow the use of half meshes. The refinement of the mesh did not appear to markedly alter the converged solution. Hence, the small quantitative differences between the current prediction and the Humphrey *et al.* measurements may be sourced to the accumulation of small errors such as omitting longitudinal diffusion of streamwise vorticity, Ω_1 (only diffusion of primary velocity, u was included), aspects of the small scalar approximation[7] remaining in the adaption of the Briley and McDonald algorithm plus contributions from non-orthogonal curvature terms omitted from the governing equations. These are clearly minor problems which may be removed with projected numerical developments in the future.

One final comment regarding the accuracy of the predictions, is related to the inability of the numerical work to predict the velocity peaks adjacent to the outer radial wall at the 60° and 90° planes. In addition to the problems outlined above, it is probable that peak primary flows are under-predicted due to numerical diffusion introduced from the first-order upwinding employed for the streamwise convection terms. Again, this is a numerical deficiency which can be corrected in the context of the multiple sweep process by second order and fourth order differencing implemented in a similar manner to that previously described for the treatment of streamwise diffusion in the axial momentum equation.

Figures 3 and *4* are longitudinal sections through the circular arc duct displaying contours of streamwise vorticity and transverse pressure correction, respectively. The streamwise vorticity development out from the side wall is shown in successive cuts at $\zeta/D_\zeta = 0.1252$ and 0.3080. At the symmetry plane ($\zeta/D_\zeta = 1.0$) the streamwise vorticity decreases to near zero towards the core of the flow. *Figure 3* indicates the generation of vorticity within the turning section and the gradual recovery of the flow in the straight exhaust. Of particular interest is the development of the vortical cell adjacent to the inner radial wall which is shown on *Figure 5* to grossly distort the primary flow. *Figure 4* displays the large adverse pressure gradients in the streamwise direction encountered at the inlet to the turning section. These cuts are taken from close to the side wall ($\zeta/D_\zeta = 0.1252$) and at the symmetry plane ($\zeta/D_\zeta = 1.0$). The distribution of the transverse pressure gradient is relatively steady in the ζ direction (into the page) but follows a large radial gradient between the inner and outer radial walls. The pressure contours also indicate the recovery of the flow in the straight exhaust in a much smaller length of duct than that required by the decay of streamwise vorticity.
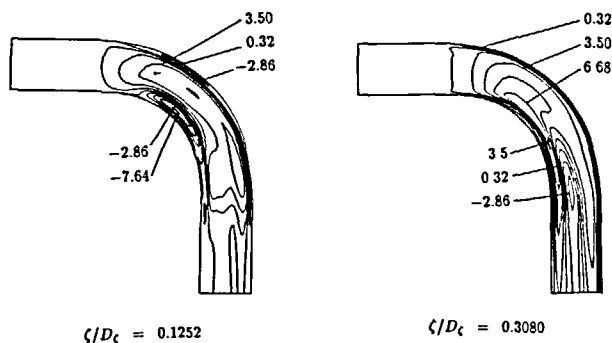

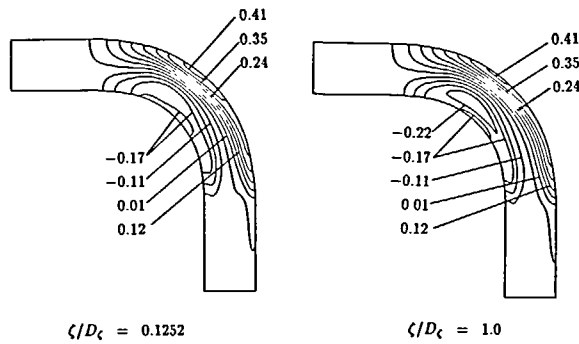Figure 3   Contours of streamwise vorticity, Ω_1 at $\zeta/D_\zeta = 0.1252$, 0.3080 for $Re = 790$

Figure 4   Contours of transverse pressure correction, Δp at $\zeta/D_\zeta = 0.1252$, 1.0 for $Re = 790$
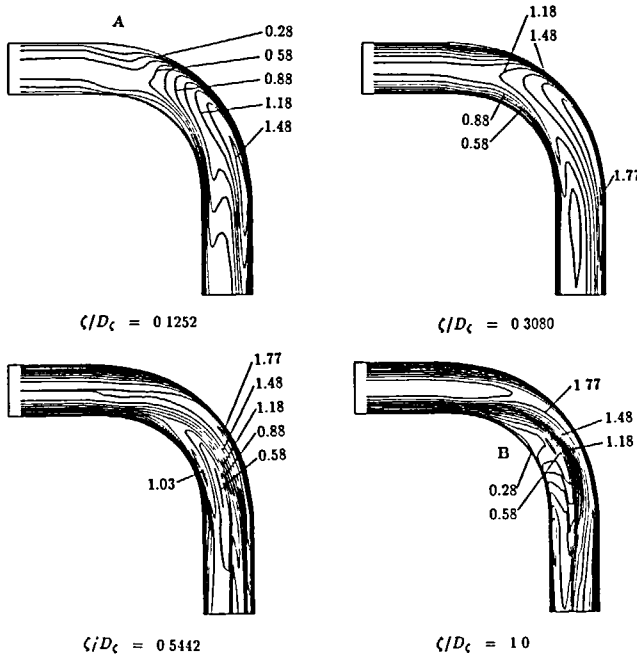

Figure 5   Contours of primary velocity, u at $\zeta/D_\zeta = 0.1252$, 0.3080, 0.5442 and 1.0 for $Re = 790$

Figure 5 displays the development of the primary velocity field throughout the turning section at successive ζ planes from near the side wall to the symmetry plane. At position A, adjacent to the outer wall and near the entrance to the bend, negative flow occurs as indicated by the distortion of the isotachs. At position B streamwise velocities fall close to zero. With increased severity of curvature, flow reversal has been predicted at this location[4] using the current code with up to peak negative velocities of $u/u_o = -0.3$. The velocity contours indicate the migration of flow towards the outer radial wall and the side walls following the rotational transverse flow generated by the curvature.

Figure 6 represents profiles of primary or streamwise velocity at the symmetry plane of straight ducts with varying aspect ratios. The laminar flow ($Re = 1000$) and turbulent flow ($Re = 1.0 \times 10^5$) in a 1:1 aspect ratio duct are profiled, comparing the parabolic shape expected from laminar
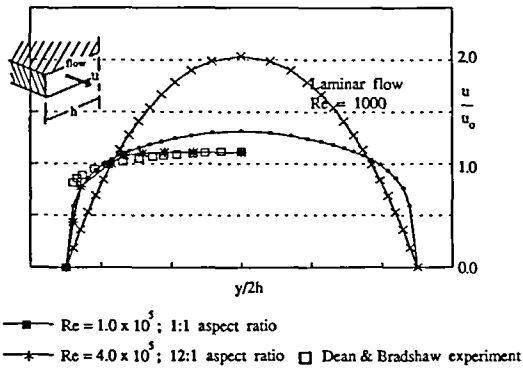
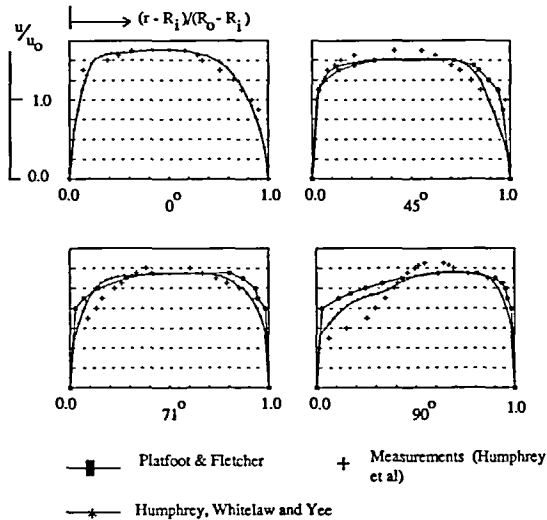Figure 6   Laminar and turbulent flow profiles at the symmetry plane of straight ducts

Figure 7   Turbulent flow $(Re=4.0\times10^4)$ in a circular arc duct with $R_i/R_o=1.8/2.8$

flow with the squarer profile of the turbulent flow's velocities. The sole numerical difference between the prediction of these flow cases is the Reynolds number and the inclusion of the eddy viscosity turbulence model previously described. The turbulence model was validated for straight duct flow with comparisons to measurements by Dean and Bradshaw[19] for a 12:1 aspect ratio duct and $Re=4.0\times10^5$. While the velocity prediction was excellent for the core flow, some discrepancy may be observed close to the side wall with the experimental measurements higher than predicted. This indicates the limitations of the zero equation model near solid walls which may be partially attributed to mesh resolution and also to the limitation of the Van Driest hypothesis as discussed by Choi et al.[3]. Despite these issues, the use of the algebraic eddy viscosity model still provides reasonable predictions of mean flow quantities as has been observed previously[21].

Figure 7 displays profiles of streamwise velocity on the symmetry plane for a turbulent flow $(Re=4.0\times10^4)$ at four different stations within the circular arc duct described above. Results from the current work are compared with the predictions and experimental measurements of Humphrey et al. The comparison is marginal for both sets of numerical results, particularly at the exit plane from the turning section. The computational predictions capture the general
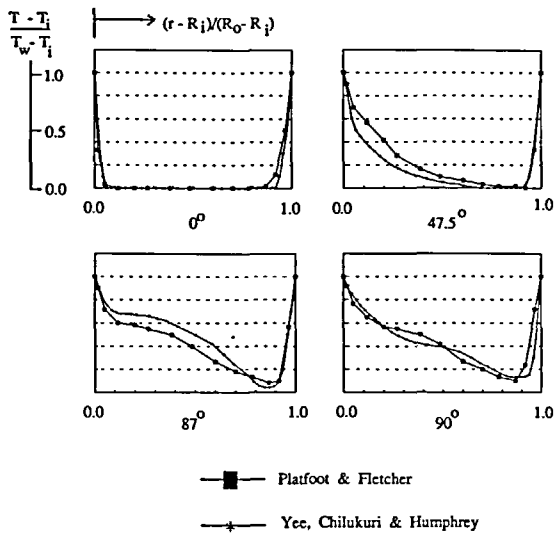
Figure 8   Laminar flow ($Re = 4.0 \times 10^4$) in a circular arc duct with $R_i/R_o = 1.8/2.8$ and heated walls

tendencies of the flow, especially the smoothing of the otherwise distorted laminar flow by the introduction of turbulence. Some migration of the flow towards the outer radial wall is evident by the 90° plane. While the current results are encouraging given the simplicity of the turbulence model and its adaption from essentially two dimensional studies to three dimensions, there is clearly need for further refinement.

The effect of the distorted laminar flow in a circular arc duct on core flow temperature is demonstrated on *Figure 8*. In this case the wall temperature is 0.167% higher than the inlet flow temperature and the Reynolds' number is 790. Profiles of normalized temperatures on the symmetry plane at four stations are presented, comparing predictions of the current work and those of Yee *et al.*[23]. The comparison indicates the similar representation of the temperature field by the two numerical models. Low velocity zones as identified in the above laminar turning flow analysis correspond to higher temperature regions downstream where the fluid is warmed by the heated walls. In this manner the temperature profiles approach an inverse form of the velocity profiles on *Figure 2*. The boundary conditions for the energy equation in the current work assumed fluid at the wall to attain the wall temperature; that is, a perfect heat transfer condition. While not physically reproducible, this condition allowed assessment of the influence of the flow structure on the temperature field. The final observation regarding the non-isothermal flow case is the absence of any strong influence on the primary flow field attributable to density gradients induced by temperature variations. This was probably due to the small temperature drop between the fluid and the perimeter wall.

CONCLUSIONS

A new multiple sweep algorithm has been developed, employing a numerically efficient marching technique within the framework of multiple forward sweeps in the direction of primary flow. This development allows complex flow cases, subject to elliptic effects, to be solved allowing downstream conditions to be accurately included as sweep-wise convergence is attained. The latter is detected when the flow solution does not significantly alter with successive marches introducing, for example, revised downstream pressure conditions. The current work considers turbulent and non-isothermal flow cases, although validation work to date suggests various areas for further refinement. However, outstanding deficiencies are associated with peripheral

modules such as the turbulence model, and the basic fluid code is completed and validated against experimental data.

The primary flow cases considered in this paper relate to turning flows within circular arc ducts and the influence of both turbulence and wall heating on the flow structure and the fluid temperature. Apart from the gross smoothing of the flow by turbulence at higher Reynolds numbers, the dominant features of the flows are the rotational influence by transverse flows induced by the curvature. A strong correspondence has been demonstrated between the distortion of the primary flow and fluid temperature distribution for the heated wall case. For the cases considered to date, no strong influence was detected due to density gradients within the non-isothermal flow. This was probably due to the small absolute thermal gradients present in the cases studied.

ACKNOWLEDGEMENT

REFERENCES

1 Rhie, C. M. A three-dimensional passage flow analysis method aimed at centrifugal impellers, *Comp. Fluids*, 13, 443–460 (1985)
2 Hur, N., Thangam, S. and Speziale, C. G. Numerical study of turbulent secondary flows in curved ducts, *J. Fluids Eng.*, 112, 205–211 (1990)
3 Choi, Y. D., Iacovides, H. and Launder, B. E. Numerical computation of turbulent flow in a square-sectioned 180 degree bend, *J. Fluids Eng.*, 111, 59–68 (1989)
4 Platfoot, R. and Fletcher, C. A. J. Computation of internal flows demonstrating severe curvature, *Int. Sym. CFD Nagoya*, Jap. Soc. CFD (1989)
5 Ghia, U., Ghia, K. N., Rubin, S. G. and Khosla, P. K. Study of incompressible flow separation using primitive variables, *Comp. Fluids*, 9, 123–142 (1981)
6 Krekovsky, J. P., Briley, W. R. and McDonald, H. Investigation of mixing in a turbofan exhaust duct; Part I: Analysis and computational procedure, *J. AIAA*, 22, 374–382 (1984)
7 Briley, W. R. and McDonald, H. Three-dimensional viscous flows with large secondary velocity, *J. Fluid Mech.*, 144, 47–77 (1984)
8 Fletcher, C. A. J. *Computational Techniques for Fluid Dynamics*, Vol. II, Springer Series in Comp. Physics, Springer Verlag, Berlin (1988)
9 Roberts, G. O. Computational meshes for boundary layer problems, *Lecture Notes in Physics, 2nd ICNMFD*, Springer Verlag, Berlin (1971)
10 Eiseman, P. R. Coordinate generation with precise controls over mesh properties, *J. Comp. Phys.*, 47, 331–374 (1982)
11 Rubin, S. G. and Reddy, D. R. Global solution procedure for incompressible laminar flow with strong pressure interaction and separation, *Comp. Fluids*, 11, 281–306 (1983)
12 Reyhner, T. A. and Flügge-Lotz, I. The interaction of a shock wave with a laminar boundary layer, *Int. J. Non-linear Mech.*, 3, 173–199 (1968)
13 Hall, E. J. and Pletcher, R. H. Application of a viscous-inviscid interaction procedure to predict separated flows with heat transfer, *J. Heat Transfer*, 107, 557–563 (1985)
14 Briley, W. R. and McDonald, H. On the structure and use of linearized block ADI and related schemes, *J. Comp. Phys.*, 34, 54–73 (1980)
15 Roach, P. J. *Computational Fluid Dynamics*, Hermosa, Albuquerque, NM (1972)
16 Cebeci, T. and Smith, A. M. O. *The Analysis of Turbulent Boundary Layers*, Academic Press, New York (1984)
17 Arnal, D. and Cousteix, J. Numerical study of corner flows, *Three Dimensional Turbulent Boundary Layers*, Springer Verlag, Berlin (1982)
18 Cebeci, T. and Chang, K. C. A general method for calculating momentum and heat transfer in laminar and turbulent duct flows, *Num. Heat Transfer*, 1, 39–68 (1978)
19 Dean, R. B. and Bradshaw, P. Measurements of interacting turbulent shear layers in a duct, *J. Fluid Mech.*, 78, 641–676 (1976)
20 Humphrey, J. A. C., Taylor, A. M. K. and Whitelaw, J. H. Laminar flow in a square duct of strong curvature, *J. Fluid Mech.*, 83, 509–527 (1977)
21 Bradshaw, P., Dean, R. B. and McEligot, D. M. Calculation of interacting turbulent shear layers: duct flow, *J. Fluids Eng.*, 94, 214–220 (1973)
22 Humphrey, J. A. C., Whitelaw, J. H. and Yee, G. Turbulent flow in a square duct with strong curvature, *J. Fluid Mech.*, 103, 443–463 (1981)
23 Yee, G., Chilukuri, R. and Humphrey, J. A. C. Developing flow and heat transfer in strongly curved ducts of rectangular cross section, *J. Heat Transfer*, 102, 285–291 (1980)